Received: 8 October 2019 | Revised: 23 March 2020 | Accepted: 5 April 2020

DOI: 10.1002/we.2515

WILEY

RESEARCH ARTICLE

Leading edge erosion of wind turbine blades: Multiaxial critical plane fatigue model of coating degradation under random liquid impacts

Saeed Doagou-Rad | Leon Mishnaevsky Jr | Jakob I. Bech

Department of Wind Energy, Risø Campus, Technical University of Denmark, Roskilde, Denmark

Correspondence
Leon Mishnaevsky Jr., Department of Wind Energy, Risø Campus, Technical University of Denmark, Frederiksborgvej 399, 4000 Roskilde, Denmark.
Email: lemi@dtu.dk

Funding information
Innovationsfonden, Grant/Award Number: 8055-00012A; Innovation Foundation of Denmark

Abstract

A computational model of rain erosion of wind turbine blades is presented. The model is based on the transient fluid–solid coupled finite element (FE) analysis of rain droplet/coating interaction and fatigue degradation analysis. The fatigue analysis of the surface degradation is based on multiaxial fatigue model and critical plane theory. The random rain fields are constructed computationally, and the estimated droplet sizes are included in FE model to acquire a library of load histories. Subsequently, the resulted nonproportional multiaxial high cycle fatigue problem is solved to assess the damage and lifetimes of the coatings. The approach can be used to design new coating systems withstanding longer service times.

KEYWORDS

coatings, erosion, rain, wind energy, wind turbine blades

1 | INTRODUCTION

Wind energy plays a critical role in this journey for a cleaner world. One approach to improve efficiency and power production of wind turbines is increasing the blade lengths. Longer blades lengths cover larger areas during rotation, which in turn increases the capacity and total potential production. For the wind turbine blades with the size of 75 m, the tip speed reaches 80 m/s.[1] However, one of the main constraints in such a development is the leading edge erosion, which plays an especially critical role for high tip speeds and can dramatically reduce blade performance particularly in the high-speed rotor tip region.[2,3] Leading edge erosion is surface degradation and removal of surface coating as the result of recurring contact of the surface with natural elements such as rain, snow, hail, and sand. In other words, energy production stopped for replacement or repair of damaged blades.[4,5] These repair and maintenance costs, combined with significant production reduction as the result of increase in the drag and decrease in the lift coefficient resulting from the erosion on the blades, present an imminent challenge.[6–8]

Interesting research has been conducted on the erosion of leading edges and their lifetimes.[9–12] However, stronger protection is required to increase the lifetime of the coatings in order to reduce aforementioned costs and delays. Therefore, the development of an efficient computational tool to assess the erosion lifetime of the coatings seems essential. However, erosion is a complex stochastic problem influenced by several critical parameters. Parameters such material properties, coating configuration, manufacturing method, and environmental conditions should be included in the model in order to attain proper results.

This paper presents a numerical methodology to estimate the erosion life and performance of coatings subjected to high-speed rain drops. The influential parameters to achieve reliable results are investigated. The presented holistic regime includes developing rain fields, finite element (FE) simulation of droplet impacts, and high cycle fatigue (HCF) calculations. Efficient connection of the mentioned numerical studies shapes a powerful tool to study the erosion behavior of the candidate materials during their service time. Moreover, the presented numerical tool is essential to develop new coatings to withstand the severe conditions.

2 | STATE OF THE ART: MODELING OF LEADING EDGE EROSION

Several analytical and computational models of leading edge erosion have been developed, from good phenomenological formulas (water hammer, damage threshold velocity; see Eisenberg et al.[10,13]) to complex multistep models[11,12] including the full model chain from turbulent flow, real rain statistics via the liquid impact,[14] up to the fatigue damage studies.[14]

The main steps of leading edge erosion modeling include the evaluation of loading (rain density, droplet size distribution, dust, and flow velocity), modeling of impact contact between droplet/particle and surface (pressure on the surface, time, deformation and damage initiation; wave distribution, Rayleigh waves), and modeling of materials degradation over time (coating cracking, debonding, cracks in composite fatigue, material loss, roughening of surface, estimation of lifetime).[4,15]

Many raindrop size distributions (DSDs) have been reported. The earliest paper on the size of raindrops backs to Laws and Parsons in 1943.[16] The different developed DSD expressions try to describe the statistical distribution of falling drop sizes specifically by representing the number of drops with a specific diameter in a unit volume of air.[17,18] Some of the mostly used raindrop size parameterization are lognormal,[19] Weibull,[20,21] exponential,[22–24] and gamma distribution.[25–27] Attaining a proper DSD at our interest area susceptible to erosion means proper application of the variability of rainfalls on the targeted surface spatially and temporally in a statistical sense. Table 1 presents different applicable DSD models and their distribution formulations. In the following studies, the distribution of rain droplets proposed by Best[28] will be used, following Amirzadeh et al.[11]

For the estimation of pressure on the coating, the analytical water hammer equation, linking pressure on the surface with the liquid impact velocity and liquid density, is widely used.[10]

Also, more complex FE models of the raindrop contact and wave propagation in the coatings have been developed. Adler et al.[29] used FE analysis to simulate water droplet impacting thick compliant coatings. The deep craters development was observed in impacted polyurethane coatings, which probably alters the evolving water drop shape. Further, it was shown that an impact by a single water droplet cannot initiate failure for polyurethane coating. Keegan and Stack[30,31] used combined Eulerian/Lagrangian approach and Explicit Dynamics tool of the FE software ANSYS, to simulate the stresses in composite and the evolution of the droplet shape. Cho[32] used Lagrangian approach to model the liquid impact and described thermodynamic states of the water by the Mie-Gruneisen equation. For the initial loading (first stage, the water drop behaves as a compressible body), water hammer pressure was estimated. For the second stage, incompressible fluid behavior, Bernoulli's stagnation pressure was used. Fraisse et al.[33] developed a FE/Abaqus model of liquid (water) and solid (resin) impact into the coated laminate and studied internal transient stresses. The target laminate was modeled using the commonly used Eulerian domain. Water droplet specified in the Lagrangian domain, where the material was not fixed to the mesh but flew through it. It was observed that at the beginning (transient stage of the impact), the highest stress is localized under the contact surface; at the quasi-static stage, the high-stress region forms in the depth under the surface. For the fatigue damage and degradation of the coatings, again, there is a rather well-justified analytical/phenomenological approach[10] and also a number of computational FE models.

Best[28] modeled interface delamination, using a cohesive zone model of coating–substrate interface. In Amirzadeh et al.[11] fatigue damage at a given point was calculated as a superposition of damages from individual raindrops. The Miner-Palmer fatigue rule and the rainflow counting were used, and the damage accumulation was calculated as proportional to time. Slot et al.[34] presented a surface fatigue model as a removal of particles detached by fatigue arising from cyclic stress variations. Again, the Miner-Palmer fatigue rule and cumulative fatigue damage equation was used. Generally, the models should include both the scenario and mechanisms of wind turbine blade degradation (in this case, rain), materials aspects (viscoelastic and damping properties of coatings, in this case), and structural task (fatigue failure of the coating, debonding). In Mishnaevsky Jr. et al.[35] the critical effect of defects (heterogeneities, particle, and voids available) in the coatings on the leading edge erosion was demonstrated. A computational model of coatings with voids and defects was presented, based on the Lagrange-Eulerian description of the droplet impact. A statistical model of erosion taking into account both the void effect and the polyurethane coating structure is developed in Mishnaevsky Jr. et al.[36] Douagou-Rad and Mishnaevsky Jr.[37] also developed 3D computational model of drop impact including the effect of surface roughness, voids, and the droplet shapes. The authors demonstrated that the smoothed-particle hydrodynamics (SPH) model of droplet

TABLE 1 Raindrop size distribution models

Model	Distribution function	Reference
Marshal and Palmer	$N(D) = N_0\, e^{-\Lambda D}, \Lambda = 4.1\, I^{-0.21}, N0 = 8000$	Marshall and Palmer[22]
Best	$F = 1 - e^{-\left(\frac{D}{1.3\, I^{0.232}}\right)^{2.25}}$	Amirzadeh et al.[11]; Marshall and Palmer[22]
Lognormal	$N(D) = \frac{N_T}{(2\pi \ln\sigma)}\, e^{-\frac{\ln^2\left(D_{D_m}\right)}{2\ln^2\sigma}}, N_T = 172\, I^{0.22}, D_m = 0.75\, I^{0.21}, \sigma = 1.45$	Feingold and Levin[19]
Ulbrich	$N(D) = N_0 D^2\, e^{-\Lambda D}$, $\Lambda = 7.09\, I^{-0.27}$, $N_0 = 64500\, I^{-0.5}$	Ulbrich[25]
Weibull	$N(D) = N_0 \frac{\eta}{\sigma}\left(\frac{D}{\sigma}\right)^{\eta-1} e^{-\left(\frac{D}{\sigma}\right)^{\eta}}, N_0 = 1000, \eta = 0.95\, I^{0.14}, \sigma = 0.26\, I^{0.42}$	Jiang et al.[21]

ensures quicker simulation as compared with the Lagrange-Eulerian description of the droplet. The procedure of numerical modeling of rain erosion was in rather general form proposed by Amirzadeh et al.[11,12] The authors of this work follow this general concept.

In summary, one can notice that there exist a number of very strong and well-justified rain scenarios and models of droplet/coating interaction. In this paper, the model for the simulation of erosion as multiaxial fatigue degradation and corresponding software is developed.

3 | COMPUTATIONAL MODEL: DROPLET DISTRIBUTION, DROPLET/COATING CONTACT MODEL, AND STRESS FIELD

The droplet/coating contact simulations were conducted using the commercial FE code ABAQUS explicit. All other computational tasks were performed using MATLAB 2019a.

3.1 | Rain field: Distribution of droplets

In order to construct rain fields for the selected DSD model, certain parameters should be known, including maximum included size of the droplet, rain intensity, speed, rain duration, and the distribution model. The combination of the area of investigation, blade tip speed, and duration of the study together constructs the volume of the study. For instance, if the area of interest on the blade is a square of 1×1 m^2 and the tip speed and rain duration are respectively 100 m/s and 10 s, the height of cube would be 1000 m with 1-m^2 cross sections perpendicular to the rain flow direction. According to the selected distribution model, the number of droplets in this volume was determined. Subsequently, the distribution of the droplet sizes was acquired by fitting the sizes to their probability. Figure 1 illustrates the distribution of the droplet sizes for the rain intensity of 10 mm/h in a period of 10 s, generated with Best distribution.

The droplets sizes were uniformly distributed in the volume of investigation. Therefore, the coordinates of each droplet with the assigned diameter were achieved. Dividing the height of each droplet coordinate over the tip speed also led to recognition of the contact times. Therefore, the coordinates of all droplets and the corresponding incident times and diameters were attained and saved to be used in the following steps.

3.2 | Droplet/coating interaction model

In order to conduct computational experiments on the coatings, 3D computational models were constructed. Coupled Eulerian-Lagrangian (CEL) method was used to solve fluid–solid interactions, following Amirzadeh et al.[11,12] The Eulerian–Lagrangian contact formulation is based on an enhanced immersed boundary method where solid part fills the void regions within the fluid domain. The contact algorithm automatically computes and tracks the interface between the Lagrangian structure and the Eulerian materials. Sensitivity analyses showed that on the basis of the size of the droplets, element size equals to 0.02 of the smallest droplet radius should be used at the initial incident area of the solid–liquid interface plane. Moreover, the box edges should be at least 10 times larger than the maximum radius of the droplet in order to capture a reliable full impact stress fields spatially and temporally. In order to capture the peak stresses and strains accurately, the first 10% of the contact period should be recorded in at least 10 steps.

Eight-node brick elements with reduced integration (C3D8R) were used as the coating layers and substrates. Moreover, one-way infinite eight-node linear elements (CIN3D8) were used on the lateral surfaces in order to avoid any reflection and interaction of stress waves from the boundary. Boundary conditions were also implemented on the bottom edges of these external faces. The general design of the models is described in detail in Douagou-Rad and Mishnaevsky Jr.[37]

In addition, fluid fields were meshed using 3D eight-node elements (EC3D8R). It is also noteworthy to mention that similar sizes of elements were used in contacting both coating surface and droplets.

Representative volume elements (RVEs) of the coating systems were constructed using the FE method in order to simulate the complex behavior of the coatings under rain droplet impacts.

The viscoelastic properties of the studied polymeric coating were determined from the performed dynamic mechanical (DMA) experiments[37] (figure 3 of Douagou-Rad and Mishnaevsky Jr.[37]). The DMA experiments were performed on a double shear specimen using a METTLER DMA (METTLER TOLEDO, USA). The extracted Prony series viscoelastic parameters from the DMA curves were used as input in the viscoelastic model in ABAQUS. Moreover, the performed uniaxial tensile experiment results were fitted into a Marlow hyperelastic model in order to capture the variation of stiffness with the undergoing strains. The stiffness of the elastic phase was used as the properties of the infinite elements. Both coatings and water were also considered nearly incompressible. The linear Us-Up Hugoniot form of the Mie-Grüneisen equation with the sound speed of 1450 m/s was used as the water equation of state.[16,19] The water density and viscosity were considered 998.2 kg/m^3 and 0.001 Pa/s, respectively.

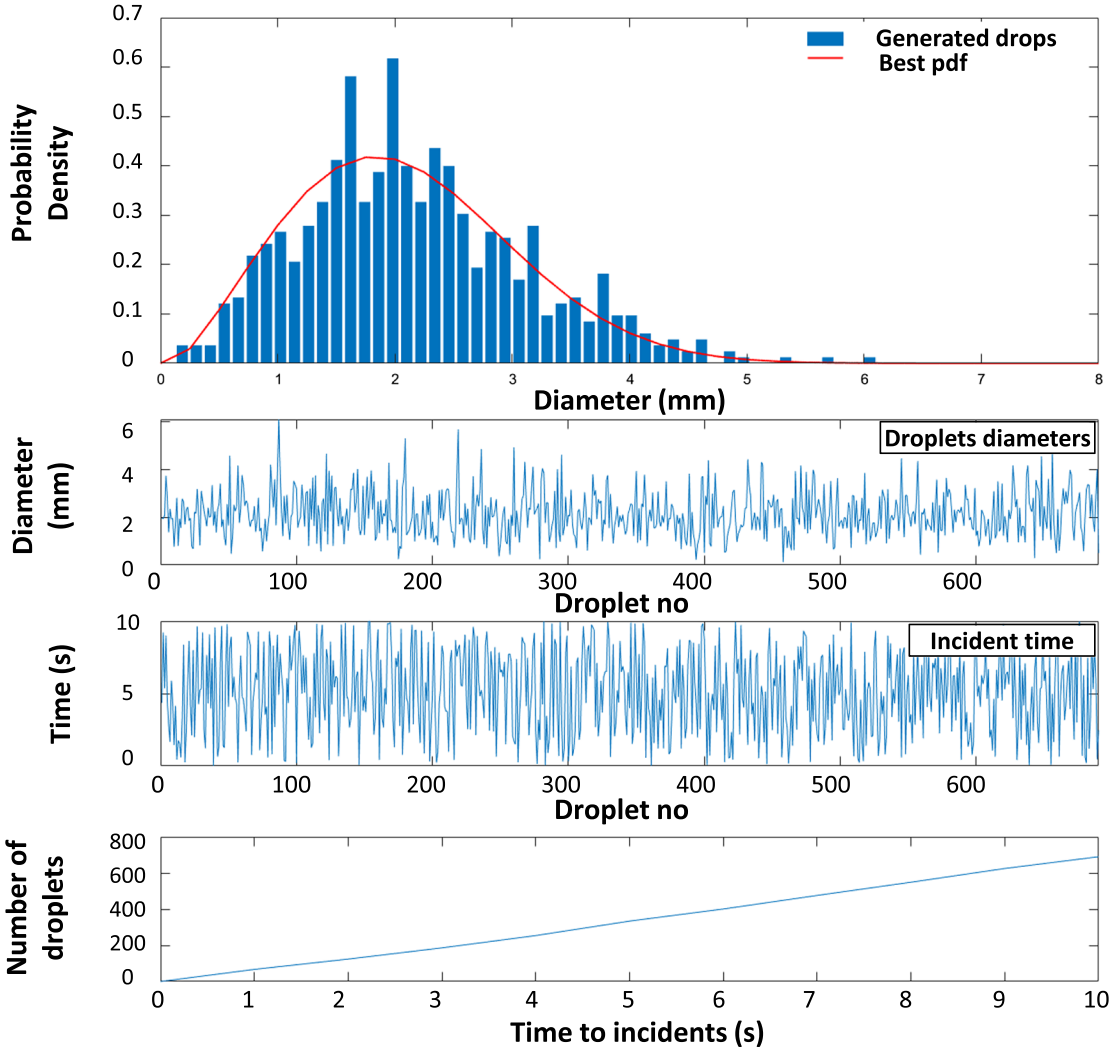

FIGURE 1 Droplet dimeter distribution for the rain intensity of 10 mm/h in a period of 10 s [Colour figure can be viewed at wileyonlinelibrary.com]

Figure 2 illustrates the sequence of the droplet shape changes and the resulting displacement fields. The duration of an incident equals to (Droplet diameter)/(Blade speed). For instance, this period becomes 10 μs for 1-mm diameter droplets hitting a blade tip with 100-m/s velocity. The maximum deformations resulting from such impact perpendicular to the surface are in the order of micrometers and retain their initial state sharply.

Figure 4 shows the distribution of shear, normal stresses, and strains as a function of distance from the impact area. One can see the clear peaks at the contours of droplet/surface contact area. It can be therefore expected that the damage can be initiated at these sites, leading to surface damage and eventually to cone, Hertzian cracks. In reality, this is not always the case, as shown in Mishnaevsky et al.[35,36] where it was observed that the damage starts very often from large defects in the coatings.

Figure 3 shows the temporal evolution of peak stress and strain as a function of time following the initial contact. One can see the drastic reduction of local stresses during 1–2 μs after the impact and then a slow reduction til 6 μs, with a quick drop afterward. Thus, the interaction with other droplet fields is to some degree possible til 6 μs after the impact. It is noteworthy to mention that the observed peaks depend on several interacting parameters including stiffness and viscoelastic properties of the surface. As it is shown in Figure 3C, the maximum strain rates reach to order of $>10^4$. Withstanding these high strain rates presents additional challenges to achieve reliable results, especially in the realm of polymeric materials where their properties vary significantly as the function of strain rates. Moreover, acquiring the required properties at high strain rates from the experiments is so expensive, challenging, unreliable, and sometimes impossible.[38] Therefore, mechanical properties are usually estimated through extrapolation of the acquired DMA results.

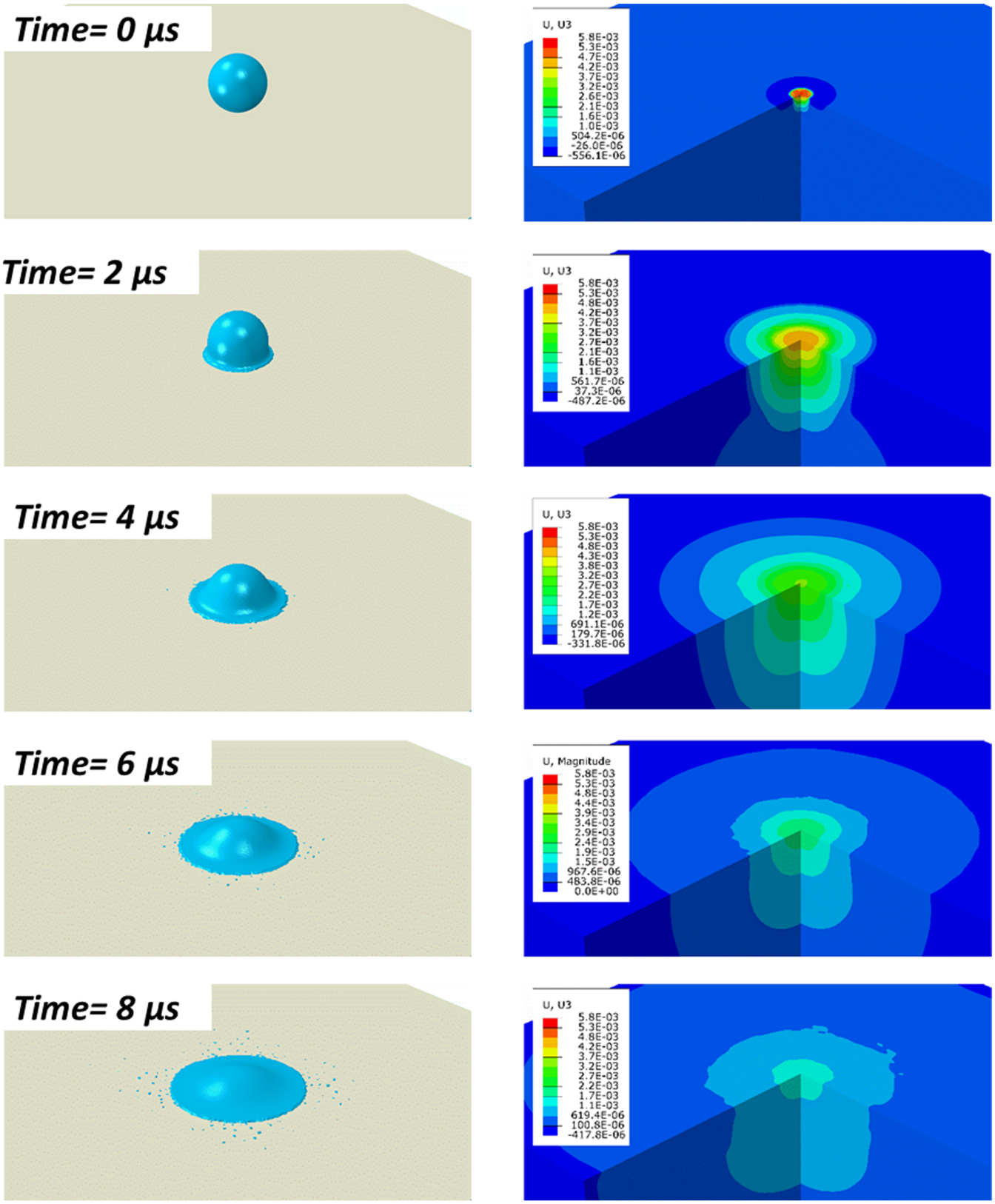

FIGURE 2 Contact interaction between droplet and the corresponding displacement fields within the coating [Colour figure can be viewed at wileyonlinelibrary.com]

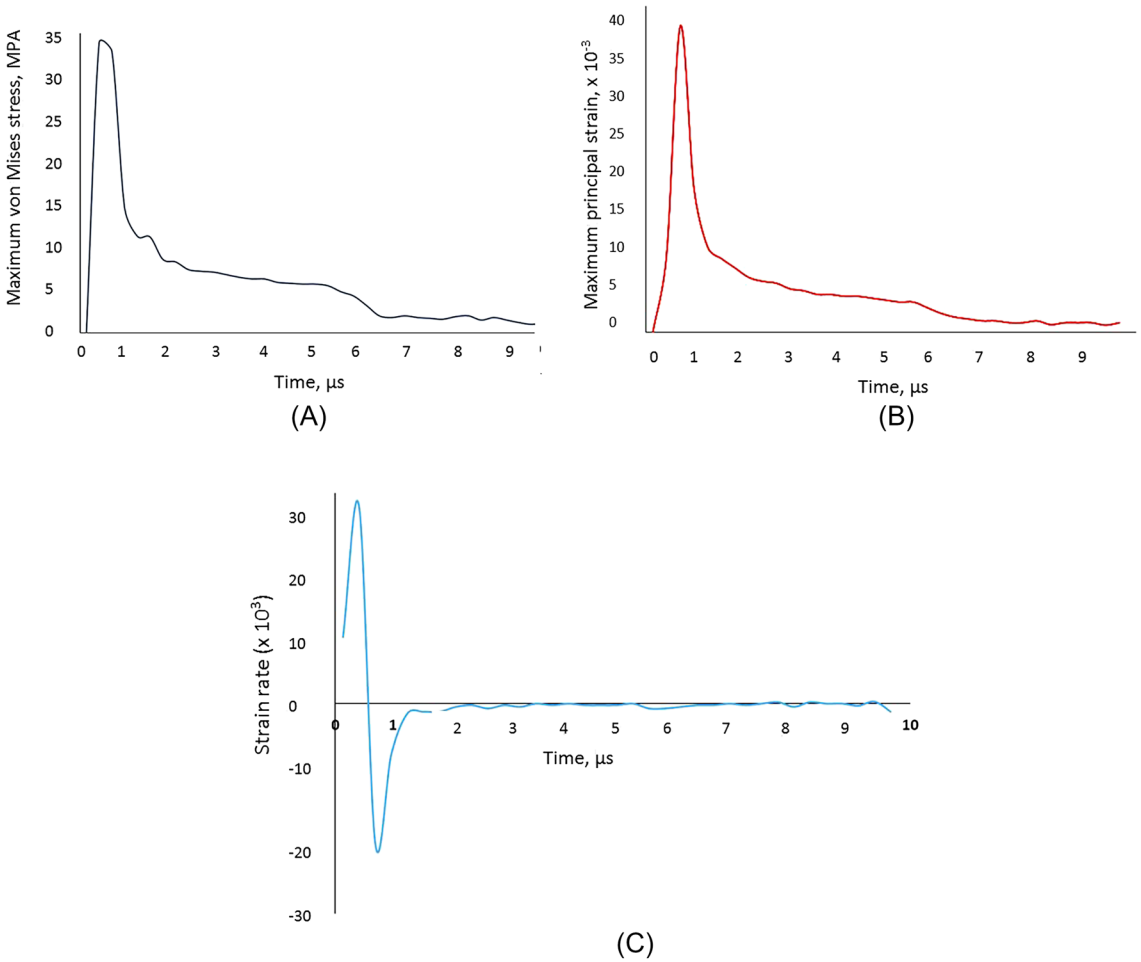

FIGURE 3 Evolution of (A) maximum von Mises stress, (B) maximum principal strain, and (C) strain rates during an impact [Colour figure can be viewed at wileyonlinelibrary.com]

3.3 | Mapping spatial and temporal evolution of stress and strain

In order to determine the load history of each point of the coating either on or below the surface, the following simulations were carried out. The rain field based on the impact speed and rain intensity has been replicated through the DSD models.

Rain droplet simulations showed that the stress waves decay in less than 1 ms.[37] The numerical simulation of the rain fields[11,37] showed that an area of 100 mm^2 under the rain intensity of 100 mm/h would see around 10 number of droplets during a sampling period of 10 s. Therefore, it can be confidently deduced that no two consecutive droplets overlap each other. This conclusion has an important influence on the further analyses, because all the achieved stress and strain values from the FE simulations could be superpositioned. As there is no interaction between the resulting waves from the incidents, each of the droplets could be studied separately, and the results are summoned and superpositioned according to their distance and time from the interest point.

Following the construction of the rain field, a sampling time is chosen. Therefore, a variation of the droplet sizes is achieved. This is the point where the constructed rain fields and FE simulations are connected in order to achieve the load history of each location of the coating under the desired period of time. In order to obtain the desired span of stress and strain through time, an interest point is chosen firstly. Subsequently, all the droplets that have influence on the state of the desired point are recognized and recorded. The area of influence was selected as circle with the radius as 10 times the largest droplet in the rain field, and all the temporal and spatial states of the droplets that fell in that region were recorded and superpositioned through the sampling period. The resulting stress and strain values of the marked droplets are summed through time. Figure 4 presents the spatial distribution of the stress and strain at one single time frame. The graphs show the range of influence of the selected droplet at every single time through the sampling period.

As described above, the stress and displacement waves decay in less than 1 ms. Therefore, all the state of stress and strain around each droplet should be recorded explicitly. In other words, stress and strain values for all integration points and at defined time steps are transferred to MATLAB. For instance, when a droplet with the size of 1 mm hits the interest point with the distance of 1.5 mm, it is known that our desired point

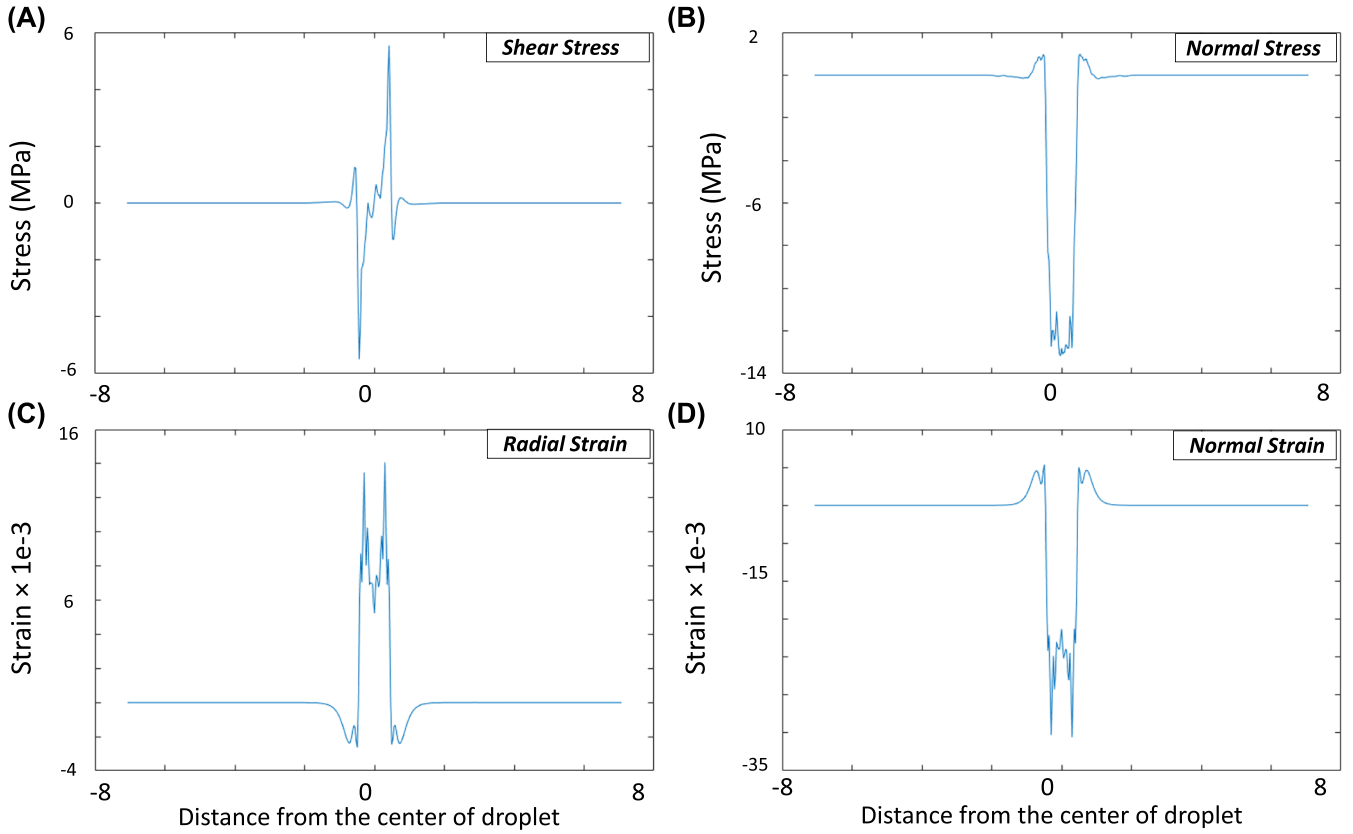

FIGURE 4 Distribution of (A) shear stress, (B) normal stress, (C) shear strain, and (D) normal strain variation as a function of distance from the contact area [Colour figure can be viewed at wileyonlinelibrary.com]

is affected by this contact. In fact, the starting and ending points of this influence accompanied with the directions and magnitudes are available. Figure 5 shows the constructed rain field as a function of time and rain intensity, as well as the distribution all of the impact locations on the surface. The rain field was obtained using the Best model as the droplet diameter variations. The 3D representation of the rain is constructed on the basis of the aforementioned input parameters (see Figure 5A). In addition, the 2D outlook of the constructed box provides all the droplet contact points through the sampling time (see Figure 5B). This 2D picture is used to map all the droplets that have influence on the interest point for the damage calculation (see Figure 5C).

Following the described procedure, the stress and strain of all the points on top and below the surface are calculated. Achieving these histories enables us to calculate the lifetime of the coatings.

4 | NONPROPORTIONAL MULTIAXIAL FATIGUE MODEL OF RAIN EROSION

4.1 | Erosion as a fatigue problem

In order to predict the erosion life of the coatings, the erosive damage is considered an HCF problem. It usually takes millions of droplet impact influences to initiate the erosion in the coatings. Therefore, the erosion of the coatings could be regarded as an HCF problem.[11,12,39] However, as described above, the area of the influence following the droplet impact is under the longitudinal and transverse waves of stress and displacement. Furthermore, the attained load histories from the superposition of stress and strain fields from a sampled rain scenario reflected the nonproportional aspects of this multiaxial state where the loadings from droplets cause a change in principal stress directions and principal stress ratio in time. Therefore, the erosion is a random nonproportional multiaxial HCF case that reflects the complexity of the problem. Although life prediction methods in the realm of uniaxial loading are established,[40,41] multiaxial variable amplitude loading, especially when the loadings are nonproportional, still needs more investigations.[42,43] In fact, multiaxial fatigue is a challenge due to the presence of a combination of interconnecting parameters including multiaxial stress state, nonproportional loading, and directional characteristics of materials and the fatigue process.[44]

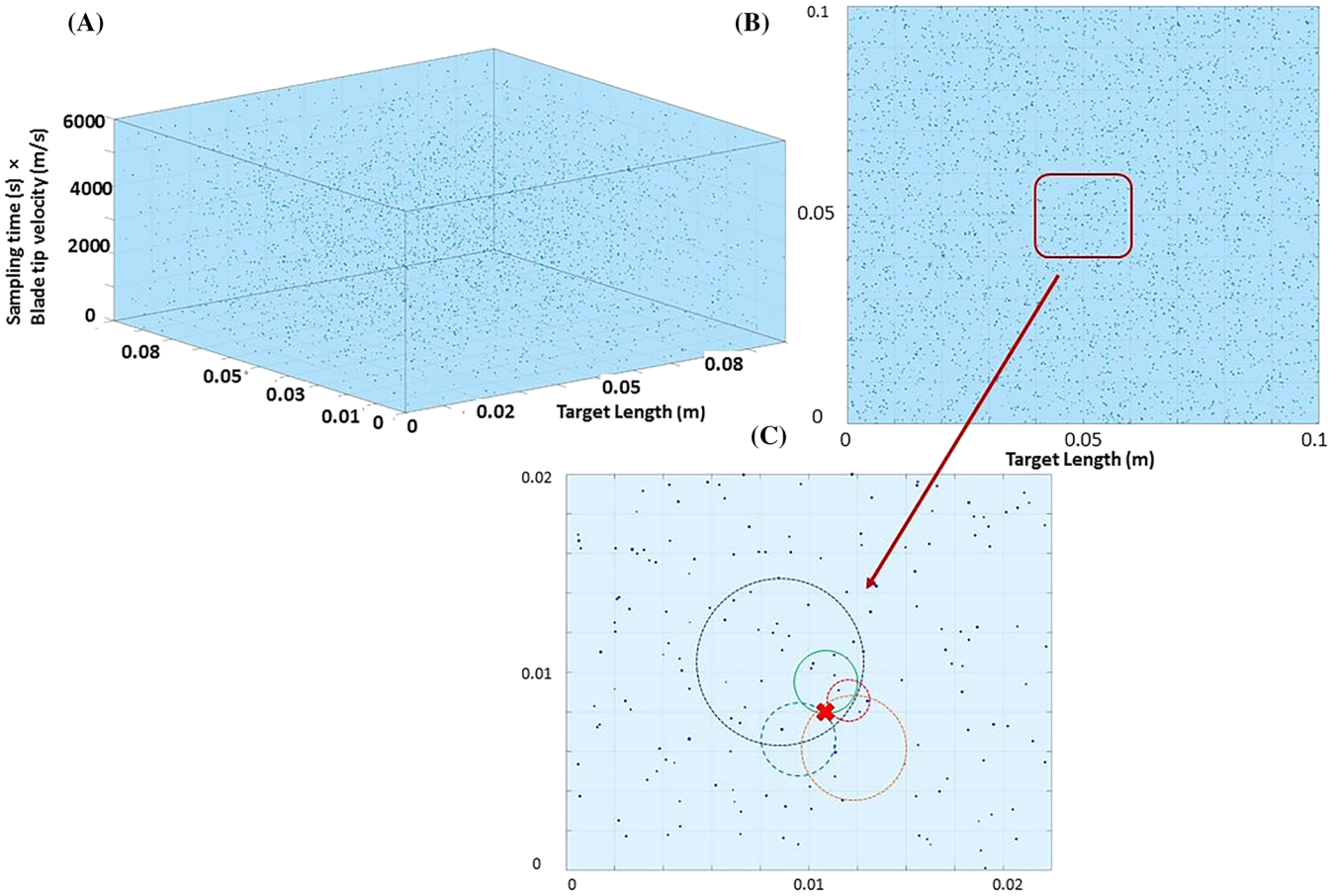

FIGURE 5 (A) Rain field as a function of time and rain intensity constructed using the Best model with varied droplet diameters. (B) Distribution all of the impact locations on the surface during the sampling period. (C) Selecting an interest point and superposition of the influencing stress fields [Colour figure can be viewed at wileyonlinelibrary.com]

4.2 | Cycle counting

Fatigue analyses require a description of the cycle count of a load sequence. Different methods such as level crossing, peak, range, and rainflow counting have been developed for this purpose.[45] Among the counting methods, rainflow counting captures the aspects the loading spectra more elaborate.[46] Following the counting, all segments of the load signal are counted as cycles, and a corresponding rainflow cycle exists for every peak in the original sequence [56.] The ASTM standard[47] was implemented as function in MATLAB.

Figure 6 presents the history of different components of stress and strain through the sampling period. The achieved load histories open the path to calculate fatigue damage according to different HCF methods.

Figure 7 shows an example of the absolute principal stress cycles and the corresponding rainflow histogram.

4.3 | Nonproportional multiaxial fatigue

Although different engineering problems are subject to multiaxial fatigue damage, their correct assessment is still challenging.[48] The fatigue calculations in these loading scenarios involve the reduction of the complex multiaxial state of stress into an equivalent parameter. However, the applied reduction criteria cannot be verified for the problem with the specific loading, material, and geometry aspects.[49] Different multiaxial fatigue models that have considered the damage problem from different perspectives have been developed. These models can be classified into three main subcategories, namely, equivalent stress, critical plane, and stress invariant-based models.

Equivalent stress methods are popular in the industry for fatigue assessment because of their simplicity, speed, and being conservative. The equivalent stress models generate one equivalent parameter from the full stress tensor. However, the effect of loading direction is eliminated in this process. Among these models, von Mises theory neglects the compressive components of stress in a loading cycle. The "signed von Mises"

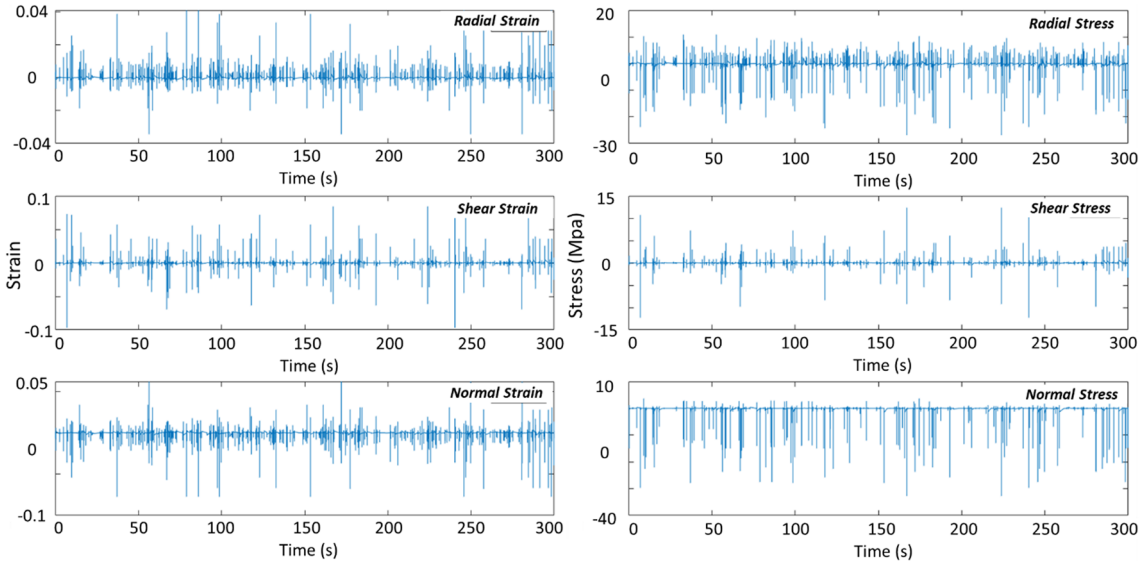

FIGURE 6 Strain and stress loading history as the result of the superpositioning impacts [Colour figure can be viewed at wileyonlinelibrary.com]

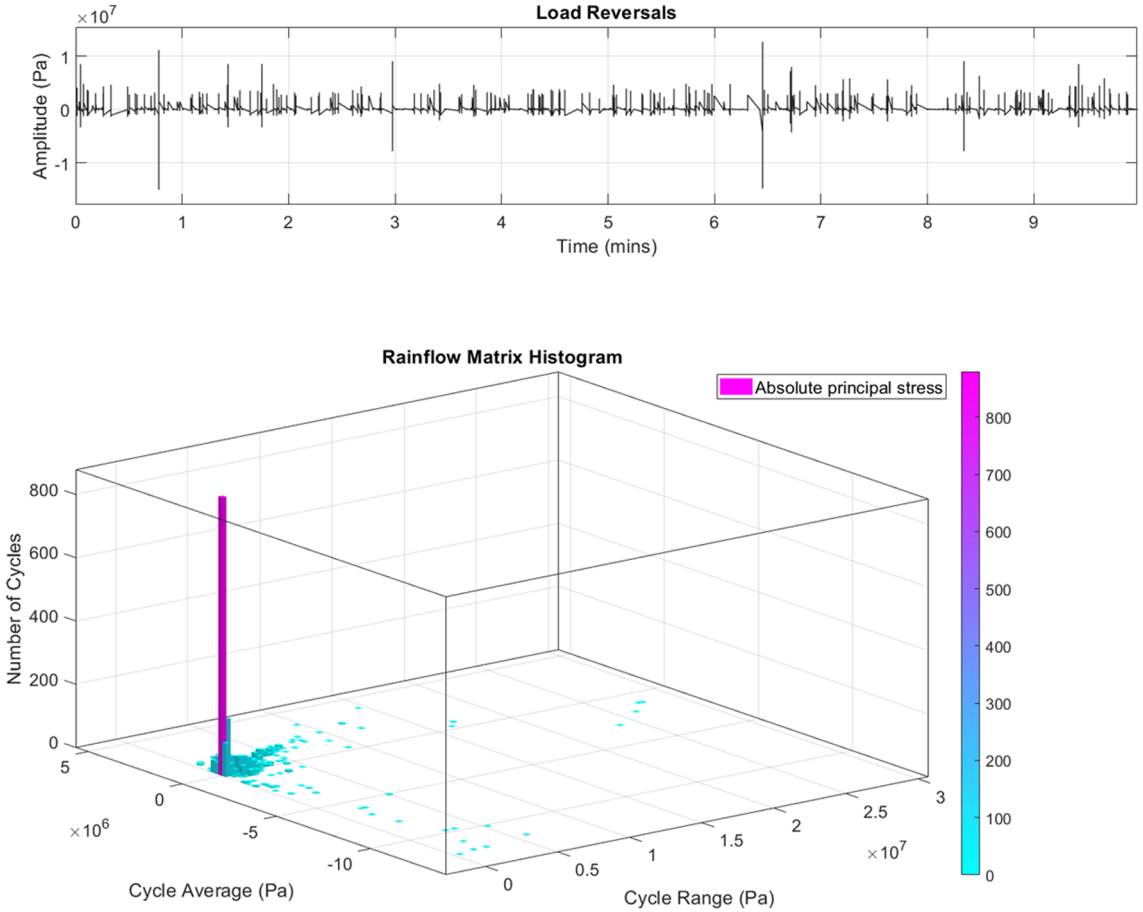

FIGURE 7 Example of the absolute principal stress cycles and the corresponding rainflow histogram [Colour figure can be viewed at wileyonlinelibrary.com]

model is an attempt to correct this drawback by application of the principal stress direction, which complicates the calculations. Furthermore, "Absolute Maximum Principal Stress" model correlates multiaxial test data by means of the static yield criteria, maximum normal stress theory. An equivalent uniaxial stress history is produced from principal stresses, and the sign of the equivalent stress at a time is the sign of the absolute

maximum principal stress. Although equivalent stress methods provide estimations that are in good agreement with test data for proportional loading, experimental studies show that they fail to account the direction of nonproportional loading and the effects of shear and tensile stresses on fatigue life. In order to cope with nonproportional loading and also considering physical mechanisms of fatigue crack initiation, the critical plane approach was used.[44,50]

The critical plane models are based on the idea that fatigue damage accumulates on a specific plane in the material, denoted the "critical plane." The damage parameter is a linear combination of shear stress and normal stress, acting on the critical plane. If applied correctly, these models are usually less conservative than the equivalent stress models. However, the determination of the critical plane often poses difficulties for the specialists.

Critical plane theories involve calculation of mean and alternating values of shear and normal stresses on every material plane to find the maximum value of a proposed damage parameter. This task could be achieved by successful coordinate transformations of the stress state and the plane where the damage parameter is maximized and subsequently is called the critical plane. In other words, the target plane is rotated in all three directions using the Euler angles, and damage is calculated on all of those rotated planes. The subsequent comparison of the acquired damage indexes reveals the maximum damage in the domain, and the corresponding plane recognized as the critical plane.

The linear damage accumulation rule, that is, "Palmgren-Miner" hypothesis, is used to predict lifetime of the coatings subjected to the discussed loadings.[51,52] "Palmgren-Miner" sum does not describe accumulation of physical damage, but the target is to estimate how many of the loading "blocks" can be applied before failure that is defined using experimental S-N curves occurs. One should keep in mind that the associated limitations of Palmgren-Miner hypothesis such as (i) being linear, (ii) neglecting potential effect of loading sequence, and (iii) being stress independent.

4.4 | Mean stress correction

The fatigue life of the coatings under the service loadings (i.e., rain droplets) depends on the amplitude of stress or strain acting in the component, but it is also influenced by the mean values of stress. In multiaxial fatigue, mean shear stress influence on the fatigue strength is normally considered in the calculations if the applied maximum shear stress is below the shear yield stress. However, the mean normal stress influences the fatigue strength explicitly, and the relationship between the fatigue strength and the static stress is assumed linear while the nominal maximum stress in a cycle is less than the yield strength.[53,54] Different relationships are applied to account for the influence of the mean stress on the material fatigue strength wherein the amplitude of the applied cyclic stress is correlated with the mean value by using either the yield or the ultimate stress. The formulation of some of these empirical relationships, namely, Gerber, Dietman, Goodman, Soderberg, and elliptical relationships, are summarized in Table. 2.[54,55]

As the mean and amplitude values of the stress are achieved for each cycle through rainflow cycle counting, the mean stress influence is addressed by using one of the mentioned relationships. Therefore, the experimental fatigue test results could be used for the life assessment of the coatings during their service time.

5 | RESULTS OF SIMULATIONS AND VALIDATION

5.1 | Damage calculation

In order to investigate the influence of the damage model on the fatigue damage assessments, three models, namely, signed von Mises, Absolute Maximum Principal Stress, and critical plane, were applied within the modeling scheme. Figure 8 illustrates the damage index distribution on the surface and depth predicted by the models. This damage mapping method allows predicting how the areas below the top surface are performing. Analyzing such figures can lead to the answer on the question on whether or not the coating is in the critical stage. In fact, as the time histories of

TABLE 2 The mean stress correction formulations

$\left(\frac{\sigma_{amplitude}}{\sigma_\infty}\right)^n + \left(f\frac{\sigma_{mean}}{\sigma_{UTS}}\right)^m = 1$	n	m	f
Soderberg	1	1	σ_{UTS}/σ_Y
Goodman	1	1	1
Gerber	1	2	1
Dietman	2	1	1
Elliptical	2	2	1

Note: σ_{UTS}, σ_Y, and σ_∞ are ultimate tensile strength, yield strength, and fully reversed axial fatigue limit, respectively.

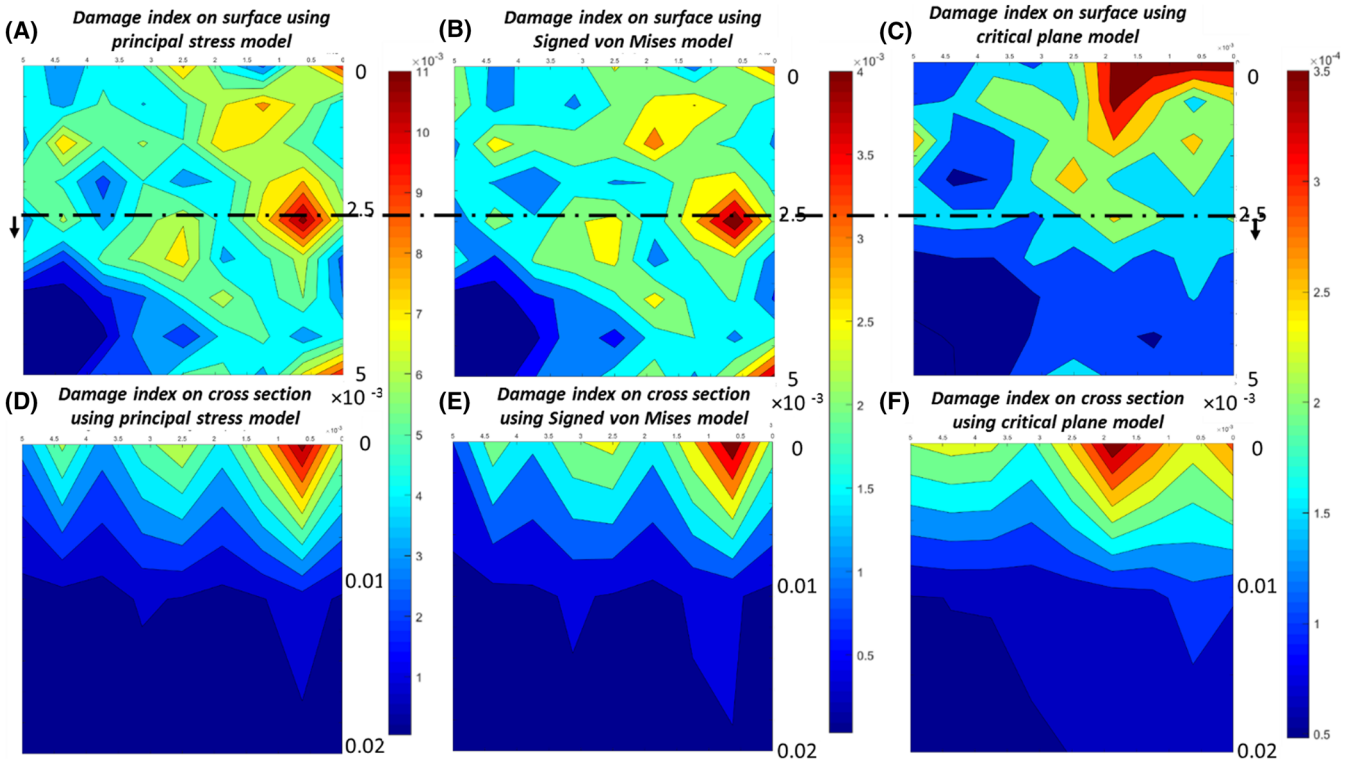

FIGURE 8 Damage on the surface based on (A) absolute principal stress, (B) signed von Mises, and (C) critical plane model. Moreover, damage through the depth based on (D) absolute principal stress, (E) signed von Mises, and (F) critical plane model [Colour figure can be viewed at wileyonlinelibrary.com]

the entire elements on and below the surface are already available, the damage could be assessed using the "Palmgren-Miner" summation.[11,12] The only difference is that different ranges of cycles are calculated through rainflow counting according to the applied fatigue model. As it can be noticed from the plotted damaged surfaces, the estimated damage using signed von Mises and absolute maximum principal stress models are one order of magnitude higher than the critical plane model. In other words, the two aforementioned models are too conservative for many applications.

Moreover, the fatigue damage evolution could be studied through the history of loading. Figure 9 presents how the fatigue damage is progressing through time. Therefore, by selection of each point on the model, the damage progress could be assessed. Acquiring such curves allows for extrapolating the results linearly to find the damage life of the desired coatings. When the damage index equals to 1.0, it is assumed that the structure has failed as the result of fatigue.

In order to investigate the influence of wind turbine blade speed (operation) and rain intensity (environment), a series of numerical investigations was performed on a sample coating. The damage on the surface and through the thickness was estimated by implementing the introduced critical plane model in the modeling regime.

A rain field with different intensities, namely, 1, 3, 6, and 10 mm/h for a duration of 10 min, was constructed (more than 150,000 droplets). The contact (leading edge) speeds of 50, 100, 150, and 200 m/s were also included in the performed modeling. The damaged surfaces were plotted within a random window of 10×10 mm^2 on the coating systems. Figure 10 presents the estimated damage rates as the function of rain intensity and blade leading edge speed. As it can be noticed from the plot, the rate of damage increases notably at higher blade speeds. Our performed FE contact simulations also showed that increasing the impact speed from 150 to 200 m/s leads to 35% increase in the peak stress values. In fact, at very high blade speeds, a few adjacent droplets could initiate damage. One might call this phenomenon a low cycle fatigue, instead of HCF. Through the described simulations, a unique damage plot could be achieved for any installed coatings. Therefore, optimum speed could be selected to achieve the highest protection rate and avoid the damage to the mounted coatings simultaneously.

5.2 | Validation

Furthermore, the reliability of the performed simulations was studied with the comparison of the achieved results with the experimental data in the literature. Experimental rain erosion tests have shown the radical influence of droplet impact speeds on the mass loss of the coatings.[56–59]

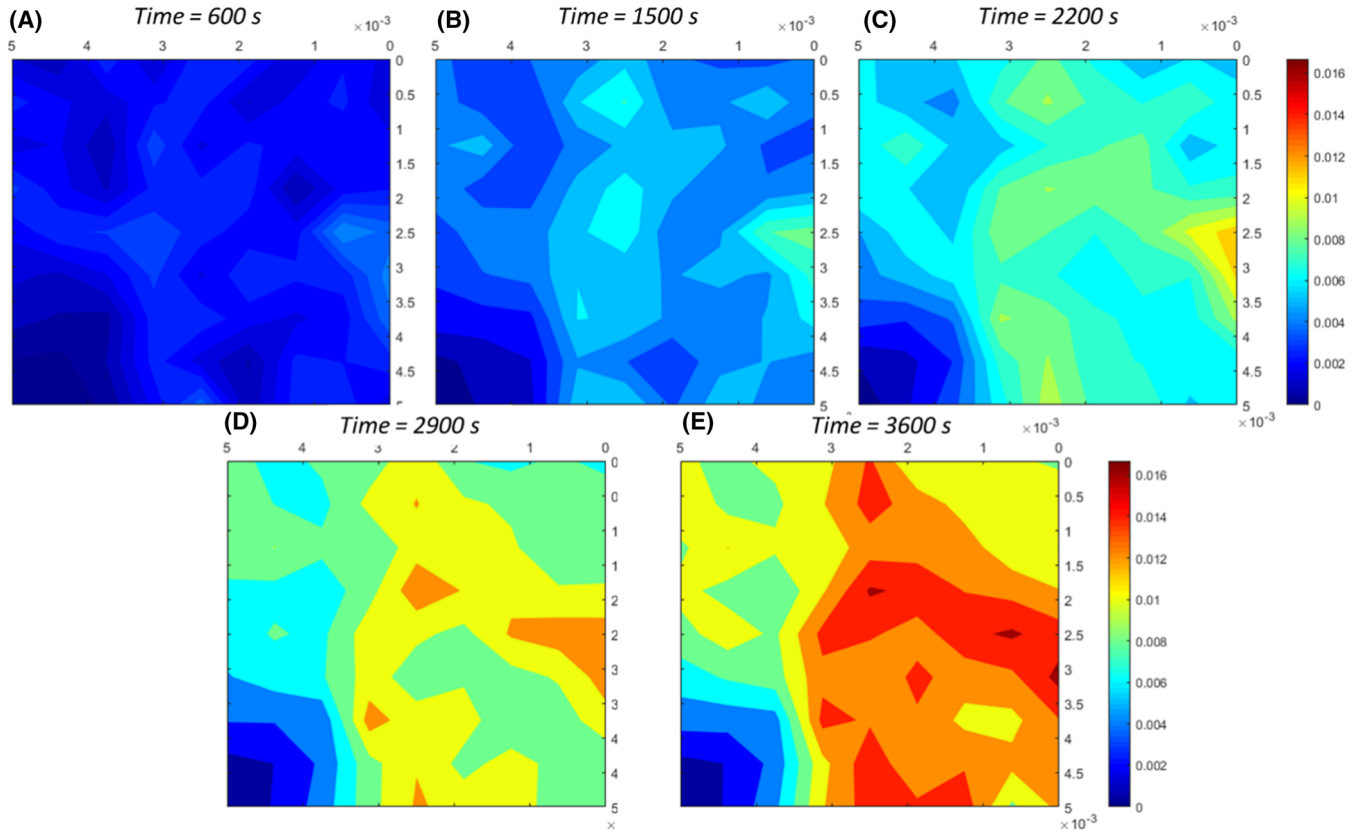

FIGURE 9 Damage evolution on the surface as the function of time [Colour figure can be viewed at wileyonlinelibrary.com]

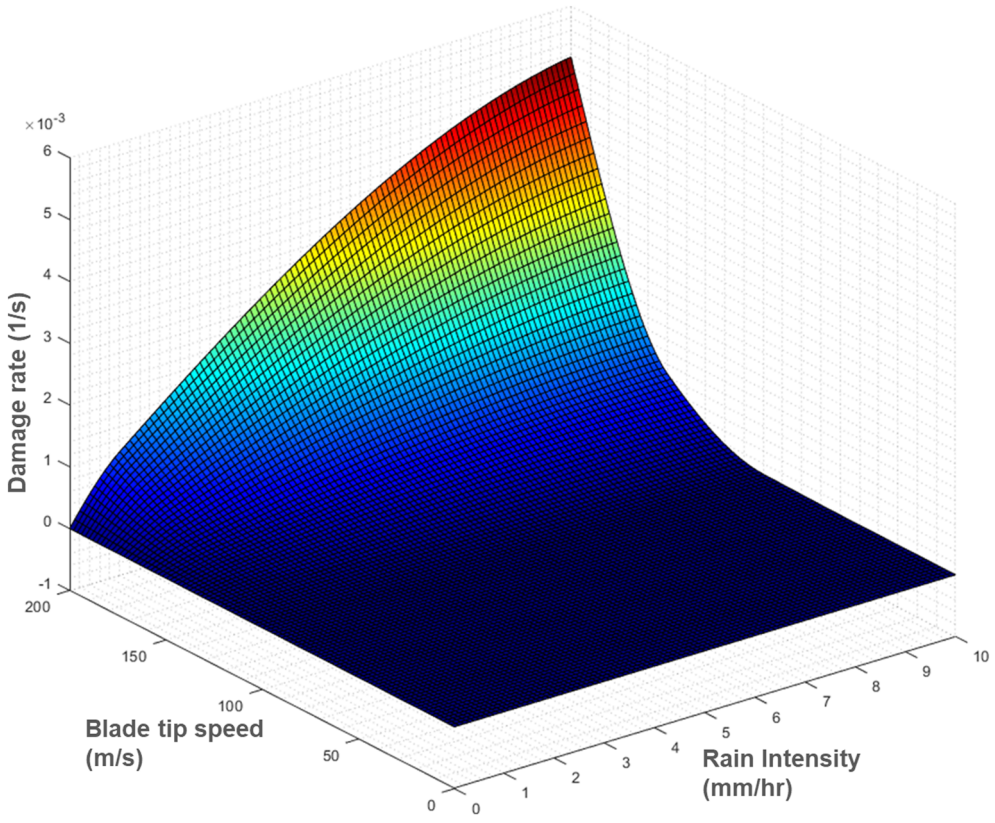

FIGURE 10 Damage rates versus blade speed and rain intensity [Colour figure can be viewed at wileyonlinelibrary.com]

Tobin et al.'s[59] experiments showed that increasing the contact speed from 180 to 225 m/s changes the coating performance drastically. Although no erosion was noticed under 180 m/s impacts, the coating specimen lost more than 140 mg under 225 m/s after 20 min of experiments. Siddons et al.[57] reported a wastage map including the measured mass loss and the impingement velocity. Their experiments showed that mass loss increases from 5 mg to more than 100 mg by increasing the contact velocity from 30 to 60 m/s. Busch et al.[58] also showed that increasing the contact speed negatively affects the performance of polymeric and metallic surfaces against erosion. They showed that increasing the contact velocities from 150 to 200 m/s leads to the loss of nearly 60% of initial weights of polymethylmethacrylate specimens within 12 minutes. Similar results were also achieved by conducting the presented simulation regime, where the damage is magnified after certain contact speeds (see Figures 10 and 11). The achieved results were also compared with the eroded surface of the wind turbine leading edges under service loads in Figure 11. In fact, the conducted simulations resulted into comparable patterns of damage to the observed eroded leading edge surfaces. Moreover, the influence of leading edge speed on the damage and their corresponding patterns is depicted.

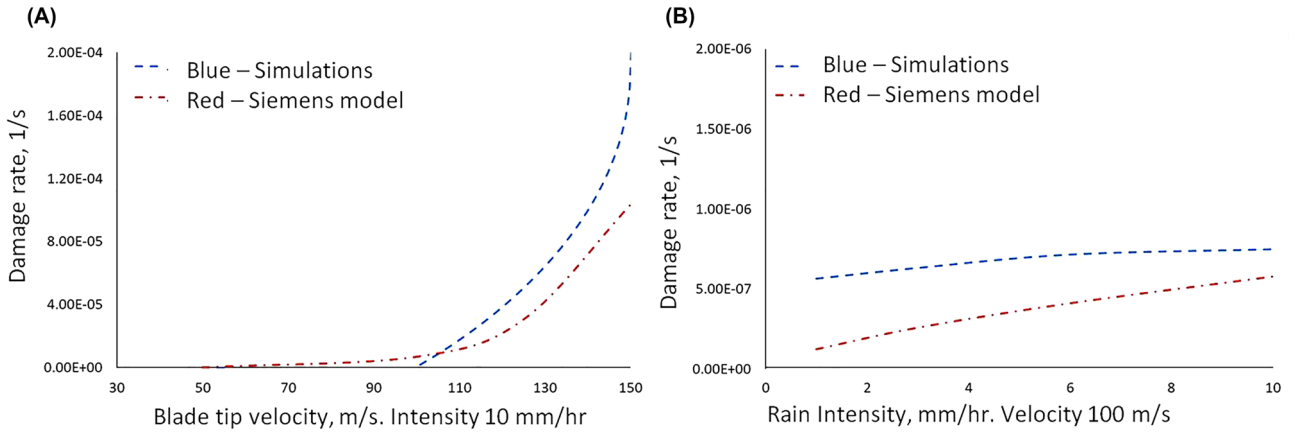

FIGURE 12 Comparison of the performed simulations with the Siemens model: influence of (A) leading edge velocity and (B) rain intensity [Colour figure can be viewed at wileyonlinelibrary.com]

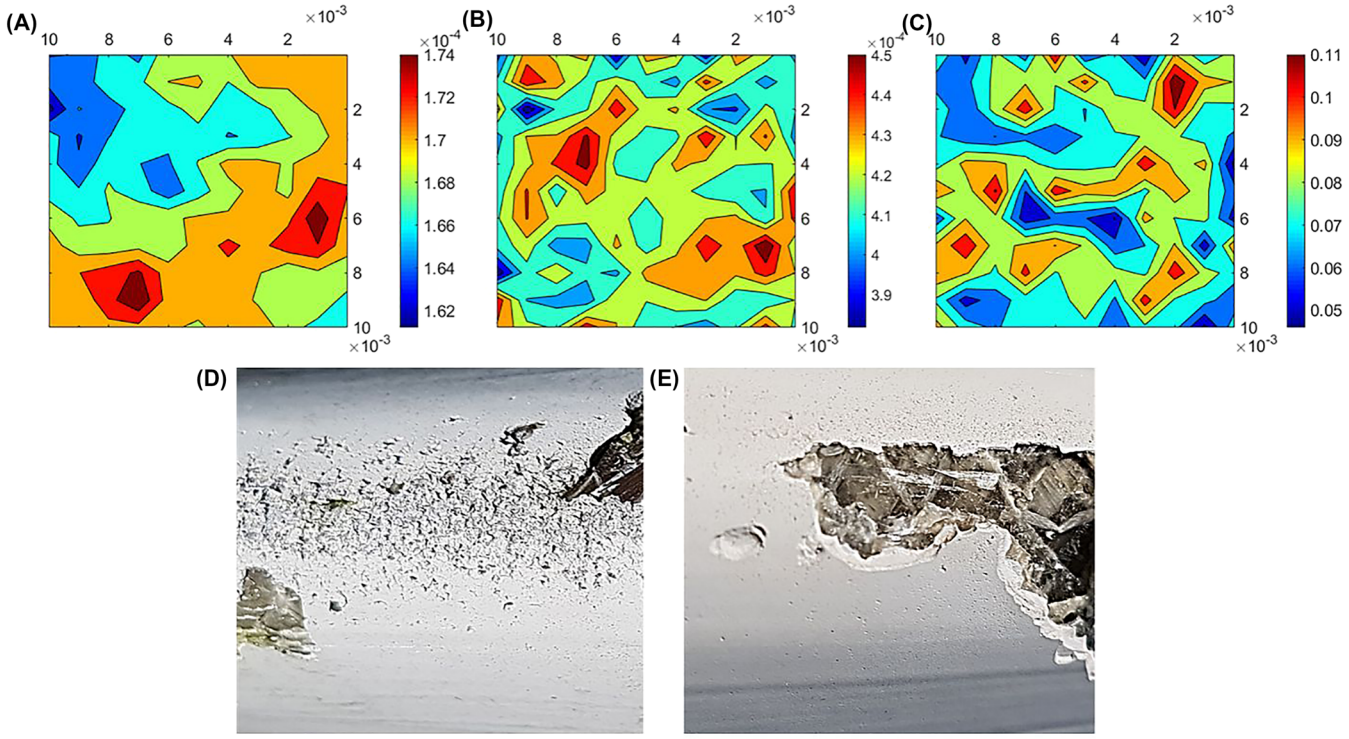

FIGURE 11 Estimated damage on the leading edge with (A) 50, (B) 100, and (C) 150 m/s speed. (D, E) The eroded surfaces of the coating under the service loads on the field [Colour figure can be viewed at wileyonlinelibrary.com]

Furthermore, the results were compared with the presented experiments and modeling by Eisenberg et al.[10] Figure 12 illustrates a comparison between the damage estimated by the described simulation regime in this paper and the empirical/theoretical Siemens model. Although there are major differences in the implemented methodologies by the two studies, the results were comparable. Eisenberg et al. used the erosion strength derived from their performed rain erosion tests, whereas in the implemented modeling regime, the standard fatigue experimental results are used. Moreover, in contrast to the performed FE simulations in this study, the pressure imposed on the surface resulting from droplet impacts are calculated from water hammer equation.[10] However, this pressure is calculated through the underlying assumption in deriving the theoretical equations wherein the impacting droplet is replaced by a liquid cylinder. Comparison of the estimated damage rates also reveals interesting findings. The implementation of the introduced simulations regime indicates less sensitivity to the rain intensity. However, it shows the critical influence of blade tip speed on the damage rate.

6 | CONCLUSIONS

A holistic simulation regime to assess the erosion life of the coating system subjected to high-speed rain droplet impacts was developed and implemented. In order to investigate the erosion performance of the coatings, several interacting parameters were investigated. The modeling regime included several consecutive steps, namely, rain field construction, FE droplet impact calculations, and nonproportional multiaxial HCF damage studies. Establishment of a proper connection between the influential elements led to a powerful erosion investigation tool, which could be used to design new durable coatings. This paper attempted to reveal the challenges and considerations that should be accounted to achieve reliable results. In essence, a reliable and realistic tool is introduced that enables life assessment of the available coatings leading to major cost reduction in inspection and maintenance of the available coatings. Moreover, the new durable protection systems could be designed, resulting into the increase of blade speeds and production rates.

ACKNOWLEDGEMENT

The authors kindly acknowledge the financial support of the Innovation Foundation of Denmark in the framework of the Grand Solutions project DURALEDGE, Durable leading edges for high tip speed wind turbine blades, File nr.: 8055-00012A.

ORCID

Leon Mishnaevsky Jr https://orcid.org/0000-0003-3193-4212

REFERENCES

1. Tarantola A. The world's biggest wind turbine, Gizmodo. 31/7/12
2. Gohardani O. Impact of erosion testing aspects on current and future flight conditions. *Prog Aerosp Sci*. 2011;47:280-303. https://doi.org/10.1016/j.paerosci.2011.04.001
3. Andersen KB. Siemens makes billions: Ørsted must have repaired hundreds of mills. Finans 2018.
4. Mishnaevsky L. Repair of wind turbine blades: review of methods and related computational mechanics problems. *Renew Energy*. 2019;140:828-839. https://doi.org/10.1016/j.renene.2019.03.113
5. Mishnaevsky L Jr. Toolbox for optimizing anti-erosion protective coatings of wind turbine blades: overview of mechanisms and technical solutions. *Wind Energy*. 2019;22(11):1-18. https://doi.org/10.1002/we.2378
6. Sareen A, Sapre CA, Selig MS. Effects of leading-edge protection tape on wind turbine blade performance. *Wind Eng*. 2012;36:525-534.
7. Gaudern N. A practical study of the aerodynamic impact of wind turbine blade leading edge erosion. *J Phys Conf Ser*. 2014;524:1-10. IOP Publishing: 12031.
8. Wood K. Blade repair: closing the maintenance gap. *Compos World*. 2011;n/a:n/a-n/a.
9. Mishnaevsky L Jr, Brøndsted P, Nijssen R, Lekou DJ, Philippidis TP. Materials of large wind turbine blades: recent results in testing and modeling. *Wind Energy*. 2012;15:83-97.
10. Eisenberg D, Laustsen SS, Stege L. Leading edge protection lifetime prediction model creation and validation. windeurope.org/summit2016
11. Amirzadeh B, Louhghalam A, Raessi M, Tootkaboni M. A computational framework for the analysis of rain-induced erosion in wind turbine blades, part I: stochastic rain texture model and drop impact simulations. *J Wind Eng Ind Aerodyn*. 2017;163:33-43.
12. Amirzadeh B, Louhghalam A, Raessi M, Tootkaboni M. A computational framework for the analysis of rain-induced erosion in wind turbine blades, part II: drop impact-induced stresses and blade coating fatigue life. *J Wind Eng Ind Aerodyn*. 2017;163:44-54.
13. Eisenberg D, Laustsen S, Stege J. Wind turbine blade coating leading edge rain erosion model: development and validation. *Wind Energy*. 2018;21:942–951.
14. Cortés E, Sánchez F, Domenech L, Olivares A, Young TM, O'Carroll A, Chinesta F. Manufacturing issues which affect coating erosion performance in wind turbine blades. AIP Conference Proceedings 1896, 030023. 2017.
15. "DURALEDGE/Durable leading edges for high tip speed wind turbine blades". File nr.: 8055–00012A, Innovation Foundation of Denmark/IFD research project, coordinated by DTU, 2018–2021. www.duraledge.dk
16. Laws JO, Parsons DA. The relation of raindrop-size to intensity. *Eos, Trans Am Geophys Union*. 1943;24:452-460.
17. Raupach TH, Berne A. Correction of raindrop size distributions measured by Parsivel disdrometers, using a two-dimensional video disdrometer as a reference. *Atmos Meas Tech*. 2015;8:343–365.

18. Bishop NWM, Sherratt F. Finite element based fatigue calculations. NAFEMS; 2000.
19. Feingold G, Levin Z. The lognormal fit to raindrop spectra from frontal convective clouds in Israel. *J Clim Appl Meteorol*. 1986;25:1346-1363.
20. Weibull W. A statistical distribution function of wide applicability. *J Appl Mech*. 1951;18:293-297.
21. Jiang H, Sano M, Sekine M. Weibull raindrop-size distribution and its application to rain attenuation. *IEE Proc-Microwaves, Antennas Propag*. 1997;144:197-200.
22. Marshall JS, Palmer WMK. The distribution of raindrops with size. *J Meteorol*. 1948;5:165-166.
23. Best AC. The size distribution of raindrops. *Q J Roy Meteorol Soc*. 1950;76:16-36.
24. Joss J, Waldvogel A. Raindrop size distribution and sampling size errors. *J Atmos Sci*. 1969;26:566-569.
25. Ulbrich CW. Natural variations in the analytical form of the raindrop size distribution. *J Clim Appl Meteorol*. 1983;22:1764-1775.
26. Atlas D, Ulbrich CW. Path-and area-integrated rainfall measurement by microwave attenuation in the 1–3 cm band. *J Appl Meteorol*. 1977;16:1322-1331.
27. Serio MA, Carollo FG, Ferro V. Raindrop size distribution and terminal velocity for rainfall erosivity studies. *A Review J Hydrol*. 2019;576:210-228.
28. Best AC. The size distribution of raindrops. *Quart J Royal Meteorol Soc*. 1950;76:16-36.
29. Adler WF, Mihora DJ. Waterdrop impact modeling. *Wear*. 1995;186:341-351.
30. Keegan N, Stack M. Modelling rain drop impact. In: ASME Turbo Expo. 2012
31. Keegan MH, Nash D, Stack M. Modelling rain drop impact on offshore wind turbine blades. *ASME Turbo Expo*. 2012;2012:1–12, Article-GT.
32. Cho J. Voronoi diagram and microstructure of weldment. *J Mech Sci Tech*. 2015;29(9):371-374.
33. Fraisse A, Bech J, Borum K, et al. Impact fatigue damage of coated glass fibre reinforced polymer laminate. *Renew Energy*. 2018;126:1102-1112.
34. Slot HM, Gelinck ERM, Rentrop C, Van Der Heide E. Leading edge erosion of coated wind turbine blades: review of coating life models. *Renew Energy*. 2015;80:837-848.
35. Mishnaevsky L Jr, Fæster S, Mikkelsen LP, Kusano Y, Bech JI. Micromechanisms of leading edge erosion of wind turbine blades: X-ray tomography analysis and computational studies. *Wind Energy*. 2019;23(3):1-16. https://doi.org/10.1002/we.2441
36. Mishnaevsky L Jr, Sütterlin J. Micromechanical model of surface erosion of polyurethane coatings on wind turbine blades. *Polym Degrad Stab*. 2019;166:283-289.
37. Doagou-Rad S, Mishnaevsky L Jr. Rain erosion of wind turbine blades: computational analysis of parameters controlling the surface degradation. *Meccanica*. 55(4):725-743. https://doi.org/10.1007/s11012-019-01089-x
38. Siviour CR, Jordan JL. High strain rate mechanics of polymers: a review. *J Dyn Behav Mater*. 2016;2:15-32.
39. Keegan MH, Nash DH, Stack MM. On erosion issues associated with the leading edge of wind turbine blades. *J Phys D Appl Phys*. 2013;46:383001.
40. Dai GM, Mishnaevsky Jr L. Fatigue of multiscale composites with secondary nanoplatelet reinforcement: 3D computational analysis, *Composites Science and Technology*, 2014;91:71–81.
41. Dai GM, Mishnaevsky Jr L. Fatigue of hybrid carbon/glass composites: 3D computational studies, *Composites Science & Technology*, 2014;94:71–79.
42. Carpinteri A, Spagnoli A, Vantadori S. A review of multiaxial fatigue criteria for random variable amplitude loads. *Fatigue Fract Eng Mater Struct*. 2017;40:1007-1036.
43. Sun G-Q, Shang D-G. Prediction of fatigue lifetime under multiaxial cyclic loading using finite element analysis. *Mater Des*. 2010;31:126-133.
44. Engin Z, Coker D. Comparison of equivalent stress methods with critical plane approaches for multiaxial high cycle fatigue assessment. *Procedia Struct Integr*. 2017;5:1229-1236.
45. ASTM standard practices for cycle counting in fatigue analysis n. d.
46. Nijssen RPL. Fatigue life prediction and strength degradation of wind turbine rotor blade composites. Contract Rep SAND2006-7810P, Sandia Natl Lab Albuquerque, NM 2006.
47. Bishop NWM, Sherratt F. *Finite element based fatigue calculations*. n/a: NAFEMS; 2000.
48. Mishnaevsky L, Brøndsted P. Statistical modelling of compression and fatigue damage of unidirectional fiber reinforced composites. *Compos Sci Technol*. 2009;69:477-484. https://doi.org/10.1016/j.compscitech.2008.11.024
49. Lorand K. Review of high cycle fatigue models applied for multiaxial tension-torsion loading based on a new accuracy assessment parameter. *J Eng Stud Res*. 2012;18:75-86.
50. Karolczuk A, Macha E. Fatigue fracture planes and expected principal stress directions under biaxial variable amplitude loading. *Fatigue Fract Eng Mater Struct*. 28(1–2):99-106.
51. Palmgren A. Die Lebensdauer von Kugellargern. *Zeitshrift des Vereines Duetsher Ingenieure*. 1924;68:339-341.
52. Miner MA. Cumulative fatigue damage. *J Appl Mech*. 1945;12:A159-A164.
53. Sines G. Behavior of metals under complex static and alternating stresses. *Met Fatigue*. 1959;1:145-169.
54. Susmel L, Tovo R, Lazzarin P. The mean stress effect on the high-cycle fatigue strength from a multiaxial fatigue point of view. *Int J Fatigue*. 2005;27:928-943.
55. Marin J. Interpretation of fatigue strengths for combined stresses. Proceedings of International Conference on Fatigue of Metals; 1956:184–94.
56. Tobin EF, Young TM, Raps D. Evaluation and correlation of inter-laboratory results from a rain erosion test campaign. Proceedings of 28th International Congress of the Aeronautical Sciences; 2012.
57. Siddons C, Macleod C, Yang L, Stack M. An experimental approach to analysing rain droplet impingement on wind turbine blade materials. EWEA 2015 Annu Event; 2015.
58. Busch H, Hoff G, Langbein G, et al. Rain erosion properties of materials. *Philos Trans R Soc London Ser A, Math Phys Sci*. 1966;260(1110):168-181.
59. Tobin EF, Young TM, Raps D, Rohr O. Comparison of liquid impingement results from whirling arm and water-jet rain erosion test facilities. *Wear*. 2011;271:2625-2631. https://doi.org/10.1016/j.wear.2011.02.023

How to cite this article: Doagou-Rad S, Mishnaevsky L Jr, Bech JI. Leading edge erosion of wind turbine blades: Multiaxial critical plane fatigue model of coating degradation under random liquid impacts. *Wind Energy*. 2020;1–15. https://doi.org/10.1002/we.2515